AJNR

Reduced Field-of-View Diffusion Imaging of the Human Spinal Cord: Comparison with Conventional Single-Shot Echo-Planar Imaging

G. Zaharchuk, E.U. Saritas, J.B. Andre, C.T. Chin, J. Rosenberg, T.J. Brosnan, A. Shankaranarayan, D.G. Nishimura and N.J. Fischbein

AJNR Am J Neuroradiol 2011, 32 (5) 813-820
doi: https://doi.org/10.3174/ajnr.A2418
http://www.ajnr.org/content/32/5/813

ORIGINAL RESEARCH

G. Zaharchuk
E.U. Saritas
J.B. Andre
C.T. Chin
J. Rosenberg
T.J. Brosnan
A. Shankaranarayan
D.G. Nishimura
N.J. Fischbein

Reduced Field-of-View Diffusion Imaging of the Human Spinal Cord: Comparison with Conventional Single-Shot Echo-Planar Imaging

BACKGROUND AND PURPOSE: DWI of the spinal cord is challenging because of its small size and artifacts associated with the most commonly used clinical imaging method, SS-EPI. We evaluated the performance of rFOV spinal cord DWI and compared it with the routine fFOV SS-EPI in a clinical population.

MATERIALS AND METHODS: Thirty-six clinical patients underwent 1.5T MR imaging examination that included rFOV SS-EPI DWI of the cervical spinal cord as well as 2 comparison diffusion sequences: fFOV SS-EPI DWI normalized for either image readout time (low-resolution fFOV) or spatial resolution (high-resolution fFOV). ADC maps were created and compared between the methods by using single-factor analysis of variance. Two neuroradiologists blinded to sequence type rated the 3 DWI methods, based on susceptibility artifacts, perceived spatial resolution, signal intensity–to-noise ratio, anatomic detail, and clinical utility.

RESULTS: ADC values for the rFOV and both fFOV sequences were not statistically different (rFOV: $1.01 \pm 0.18 \times 10^{-3}$ mm^2/s; low-resolution fFOV: $1.12 \pm 0.22 \times 10^{-3}$ mm^2/s; high-resolution fFOV: $1.10 \pm 0.21 \times 10^{-3}$ mm^2/s; $F = 2.747$, $P > .05$). The neuroradiologist reviewers rated the rFOV diffusion images superior in terms of all assessed measures ($P < 0.0001$). Particular improvements were noted in patients with metal hardware, degenerative disease, or both.

CONCLUSIONS: rFOV DWI of the spinal cord overcomes many of the problems associated with conventional fFOV SS-EPI and is feasible in a clinical population. From a clinical standpoint, images were deemed superior to those created by using standard fFOV methods.

ABBREVIATIONS: ADC = apparent diffusion coefficient; AP = anteroposterior; DTI = diffusion tensor imaging; DWI = diffusion-weighted MR imaging; EPI = echo-planar imaging; fFOV = full FOV; HiRes, high resolution; isoDWI = isotropic DWI; LoRes, low resolution; RF = radio frequency; rFOV = reduced FOV; ROI = region of interest; SNR = signal intensity to noise ratio; SS-EPI = single-shot EPI; STIR = short tau inversion recovery; ZOOM-EPI = zonal oblique multisection EPI

SPINE

ORIGINAL RESEARCH

DWI of the spinal cord is rarely performed clinically, because it is difficult to obtain distortion-free, high-resolution images by using standard SS-EPI.[1-5] Interest in spinal cord DWI is increasing, however, because it is expected to be useful in a diverse range of pathology, including demyelinating disease,[6-9] infarction,[10-15] myelopathy,[16-19] and traumatic injury.[20-23] Furthermore, diffusion images serve as the raw data for DTI,[9,19,23-29] which enables the mapping of white matter tracts; this could improve clinical management of pathologies such as neoplasms and spinal cord injury.

Standard SS-EPI is prone to distortions, primarily because of its long readout time and low bandwidth in the phase-encode direction.[30,31] Thus, prior investigators have developed EPI-based and other methods that address this issue, including navigated fast spin-echo,[3] line scan imaging,[32-35] propeller-based imaging,[36-38] and interleaved[4,39,40] and parallel EPI[28,41,42] approaches. For all of the non-single-shot approaches, readouts from several excitations are combined to create the final image; this incurs penalties in scan time and requires compensation for dephasing due to patient motion during diffusion-sensitizing gradients. Parallel EPI avoids the motion issues but suffers from decreased SNR per unit time and requires specialized imaging coils, because most commonly used spine coils are not lined up along the direction of phase-encoding and render parallel MR imaging infeasible. More recently, methods aimed at reducing the effective FOV have been suggested, including both outer volume suppression and inner volume excitation.[19,43-47] These methods are attractive because of the geometry of the spinal cord, which enables a significant FOV reduction in the AP direction.

Here, we describe our experience with an rFOV diffusion method that uses a 2D echo-planar RF pulse to excite and subsequently read out a rectangular-shaped FOV.[45] Similar to interleaved or parallel EPI, this permits a faster *k*-space traversal for a given spatial resolution, without ghosting or residual aliasing and reduces artifacts associated with fFOV SS-EPI. In addition, the excitation scheme allows inherent fat suppression, which is particularly important for EPI-based imaging. The purpose of the current study is to evaluate the performance of rFOV spinal cord

Received July 21, 2010; accepted after revision October 6.

From the Departments of Radiology (G.Z., J.B.A., J.R., T.J.B., N.J.F.) and Electrical Engineering (E.U.S., D.G.N.), Stanford University, Stanford, California; Department of Radiology (C.T.C.), University of California–San Francisco, San Francisco, California; and Applied Sciences Laboratory-West (A.S.), GE Healthcare, Menlo Park, California.

A.S. is a full-time employee of GE Healthcare. The remaining authors who are not employees of GE Healthcare had control of inclusion of any data and information that might present a conflict of interest for this author.

Please address correspondence to Greg Zaharchuk, PhD, MD, 1201 Welch Rd, PS-04, Stanford University Medical Center, Mailcode 5488, Stanford, CA 94305-5488; e-mail: gregz@stanford.edu

Indicates article with supplemental on-line figures.

DOI 10.3174/ajnr.A2418

DWI and compare it with the routine fFOV SS-EPI method in a clinical population.

Materials and Methods

Industrial Support

The pulse sequence used is a collaborative "work-in-progress" between Stanford University and General Electric Healthcare.

Patient Population

MR imaging studies were acquired as part of routine clinical care. All patients provided written informed consent approved by our institutional review board for a prospective study of the safety and utility of advanced imaging sequences between March and July 2009. Patients with cervical spine examinations performed at 1.5T for clinical purposes were enrolled in the study. Three different magnets (Signa, GE Healthcare, Waukesha, Wisconsin; 40 mT/m maximum gradient strength and 150 mT/m/ms maximum slew rate) were used. Thirty-six patients (18 males, 18 females; mean age, 52 ± 19 years; range, 17–85 years) met the entry criteria. Imaging indications were similar to those that are routine at our institution (posttrauma, $n = 11$; neck pain, $n = 7$; known or suspected neoplasm, $n = 4$; weakness, $n = 3$; sensory abnormalities, $n = 3$; combined weakness and sensory abnormalities, $n = 3$; prior examination with incidental finding, $n = 2$; neurodegenerative disease, $n = 1$; known or suspected infection, $n = 1$; postsurgical follow-up, $n = 1$).

Imaging Methods

For all studies, the built-in body volume coil was used for signal intensity transmission and an 8-channel cervical-thoracic-lumbar coil for signal intensity reception. All patients received standard anatomic imaging of the cervical spine, which at our institution includes sagittal T1-weighted (TR/TE, 500/22 ms), sagittal T2-weighted fast spin-echo (TR/TE, 2400/115 ms), sagittal STIR (TR/TE/TI, 4615/50/140 ms), axial T2-weighted fast spin-echo (TR/TE, 4500/103 ms), and axial gradient-echo (TR/TE. 475/11 ms) images.

The diffusion-weighted spin-echo rFOV SS-EPI images were acquired in the sagittal plane, by using six 4-mm sections with no intersection gap. The rFOV was achieved by a 90° 2D echo-planar RF excitation followed by a refocusing 180° pulse. A full description of the method can be found in Saritas et al,[45] and a pulse sequence diagram is included in On-line Fig 1. TR/TE/EPI readout time was 3600/69/54 ms. $b = 0$ images as well as $b = 500$-s/mm^2 images acquired in 3 orthogonal planes were acquired. Lower than normally used in the brain, this b-value was chosen due to the high ADCs in the white matter along the cephalocaudal direction, as well as the decreased SNR due to the high in-plane resolution. The rFOV was 18 × 4.5 cm^2, which with a matrix of 192 × 48, yielded in-plane spatial resolution of 0.94 × 0.94 mm^2. Two additional comparison DWI sequences were performed by using fFOV SS-EPI imaging, with a square FOV of 18 cm^2, by using the same section thickness and locations. fFOV diffusion-weighted images were acquired either with the same spatial resolution as the rFOV images (192 × 192 matrix, 0.94 × 0.94 mm^2 in-plane resolution), which led to an increased TE and longer readout time (TR/TE/EPI readout time, 3600/102/216 ms), or with preserved readout time and subsequent lower spatial resolution (96 × 96 matrix; 1.92 × 1.92 mm^2 in-plane resolution; TR/TE/EPI readout time, 3600/70/54 ms). Partial k-space acquisition of 62.5% was used to shorten TE, and complex signal intensity averaging after phase correction was performed such that all 3 sequences had the same acquisition time (2.5 minutes). Neither respiratory nor cardiac gating was used for any of the sequences. Details of each of the sequences are included in Table 1. Postprocessing software automatically produced isoDWI and ADC images by using standard methods, which were available for immediate review.

Table 1: Imaging parameters for the DWI sequences

	rFOV	LoRes fFOV	HiRes fFOV
TR/TE (ms)	3600/69	3600/70	3600/102
FOV (frequency × phase encode) (cm)	18 × 4.5	18 × 18	18 × 18
Matrix size	192 × 48	96 × 96	192 × 192
Bandwidth (Hz/pixel, kHz)	62.5	62.5	62.5
Readout time (ms)	54	59	216
In-plane resolution (mm)	0.9 × 0.9	1.9 × 1.9	0.9 × 0.9
Section thickness (mm)	4	4	4
Acquisition time (min:s)	2:30	2:30	2:30

Although not part of the comparison study, 3 additional patients had rFOV imaging performed and findings are presented in the on-line material as examples of axial DWI of the cervical cord and sagittal thoracic spinal cord diffusion in patients with and without pathology. Axial imaging of the cervical spine was performed in a 53-year-old man with a history of trauma (On-line Fig 2). Parameters for this scan were as follows: TR/TE, 3600/64 ms; FOV, 16 × 4 cm^2; matrix, 192 × 48; voxel size, 0.83 cm^2; and 6-mm section thickness with 1.5-mm skip. Thoracic spinal cord imaging is presented in 2 patients: a 49-year-old man scanned to evaluate known nerve sheath tumors (On-line Fig 3); and an 57-year-old man with known type B aortic dissection, and more recent history of acute onset paraparesis and chest pain radiating to back (On-line Fig 4). Sagittal rFOV imaging with the following parameters was performed in both of these patients: TR/TE; FOV, 30 × 6 cm; matrix, 320 × 64; and voxel size, 0.94 cm^2. In the first patient, an additional fFOV scan was performed by using the following parameters: TR/TE, 3000/69 ms; FOV, 30 cm^2; matrix, 128 × 128; and voxel size, 2.3 cm^2.

Radiologic Assessment

IsoDWI and ADC images from the 3 different DWI sequences were blinded and placed in random order by using a Fisher-Yates shuffle. Two neuroradiologists, each with >15 years of academic experience (C.T.C. and N.J.F.), evaluated each of the sequences (rFOV, low-resolution fFOV, and high-resolution fFOV) on the following imaging characteristics: anatomic detail, susceptibility and/or susceptibility-induced artifacts; perceived spatial resolution; perceived SNR; and perceived clinical utility. Scoring was performed based a 5-point scale as follows[37,48]: 1 = nondiagnostic, 2 = poor, 3 = satisfactory, 4 = good, and 5 = excellent.

Another neuroradiologist (J.B.A.) manually outlined circular ROIs on the midline sagittal image with an area and volume of 0.19 cm^2 and 0.77 cm^3, respectively, to compare ADC values among the different sequences. This size was chosen to be small enough to be placed within the cervical cord on all images regardless of field inhomogeneity-induced distortion, which often narrowed the apparent cord diameter on fFOV images, but to be large enough to obtain a reasonable number of voxels with which to calculate ADC (22 voxels for the rFOV and high-resolution fFOV and 5 voxels for the low-resolution fFOV). ROIs were placed immediately posterior to the inferior aspect of the C2 vertebral body such that the ROI was tangent and superior to a line drawn parallel to and passing through the C2–3

disk space. This location was chosen because it was relatively free of distortion and artifacts regardless of the acquisition technique, sequence, patient body habitus, or position within the scanner.

Statistical Analysis

All statistical analyses were performed by a biostatistician (J.R.) using Stata release 9.2 (StataCorp, College Station, Texas). ADC was compared among the 3 diffusion scans by using single-factor analysis of variance, and $P < .05$ was considered significant. Agreement between readers was assessed with weighted κ and exact Bowker test of symmetry. Pair-wise comparisons of neuroradiologist reviewers' evaluations of the different DWI sequences were done with paired Wilcoxon tests.

Results

No abnormal findings, including reduced or increased diffusion, were noted in the patients included in this study, with the exception of varying degrees of degenerative disk disease. T2-weighted anatomic images, rFOV isoDWI, and ADC maps are shown for a representative case in Fig 1. We observed improvements in imaging artifacts by using rFOV isoDWI compared with our standard low-resolution fFOV isoDWI, particularly distortions in the phase-encode direction (AP on our images). An example of this is shown in Fig 2, in which the rFOV method has improved anatomic appearance compared with either of the fFOV methods. The fFOV images demonstrate pixel misregistration in the AP direction due to susceptibility. Also, artifacts seen at the edges of the disks and the CSF space of the spinal canal are significantly reduced on the rFOV images. Due to the prolonged readout with the high-resolution fFOV SS-EPI, T2*-induced blurring is also much stronger than on the rFOV scans with identical spatial resolution.

An example of axial imaging of the cervical spinal cord is shown as On-line Fig 2. Although fFOV diffusion images were not acquired in this patient, the general quality of the images are comparable or better than the typical scans acquired at our institution by using fFOV. For the purposes of example, a single comparison of rFOV and fFOV diffusion imaging of the thoracic cord is shown in On-line Fig 3. The higher resolution and reduced distortion has enabled the visualization of a small central CSF cavity in the distal thoracic cord, the terminal ventricle, which is not evident on the fFOV images. A further example of thoracic spinal cord diffusion imaging is shown in On-line Fig 4 that also demonstrates high signal intensity on DWI with associated low ADC in the central cord in the lower thoracic spine consistent with acute spinal cord infarct.

Figure 3 shows the location of the ROI in which the ADC measurements were made. The ADC values obtained with the rFOV approach were not statistically different from either of the fFOV diffusion techniques (rFOV, $1.01 \pm 0.18 \times 10^{-3}$ mm^2/s; low-resolution fFOV, $1.12 \pm 0.22 \times 10^{-3}$ mm^2/s; high-resolution fFOV, $1.10 \pm 0.21 \times 10^{-3}$ mm^2/s; $F = 2.747$, $P > .05$). There is reduced interpatient variance for the rFOV method that may be related to the improved anatomic fidelity of the images.

Agreement between the 2 neuroradiologist reviewers was moderate to good (Table 2). The readers did not show a tendency to over- or underscore compared with each other, except for the category of anatomic detail, in where reviewer 2 gave higher ratings overall compared with reviewer 1 ($P = .011$). The reviewers preferred the rFOV images by a strong margin in all metrics (Fig 4). All 3 sequences were significantly differently from one another on all ratings, with rFOV having consistently higher ratings than the low-resolution fFOV sequence, which in turn was preferred compared with the high-resolution fFOV sequence (all calculated P values $\leq .0001$) (Fig 4). This was most pronounced for the preference of the rFOV method on the basis of reduction of susceptibility artifacts, in which the rFOV images were scored good or excellent 69% of the time, compared with 7% for either of the fFOV images. Likewise, clinical utility was deemed excellent 51% of the time for the rFOV diffusion images versus 1% for either of the fFOV methods. Improvements in anatomic fidelity are illustrated by the case of a patient with left-sided arm weakness and multiple posterior disk-osteophyte complexes, the largest of which is at C4–5; the fFOV images demonstrate significant misregistration and image degradation in the regions of the osteophytes, which is largely alleviated by the rFOV approach (Fig 5). Another case of a patient with a C6–7 anterior cervical

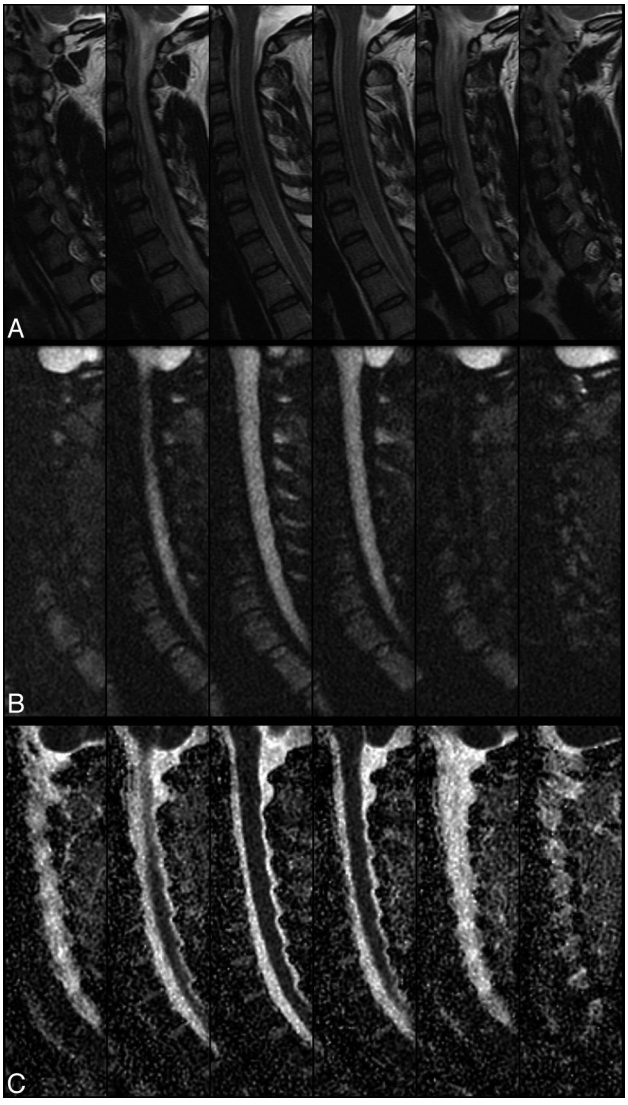

Fig 1. A 35-year-old woman status postmotor vehicle crash with neck pain and bilateral upper extremity numbness and tingling. Sagittal T2-weighted (*A*), rFOV diffusion-weighted images (*B*), and rFOV ADC maps (*C* are shown). Typically, six 4-mm contiguous sections were acquired, covering the entire extent of the cervical spinal cord.

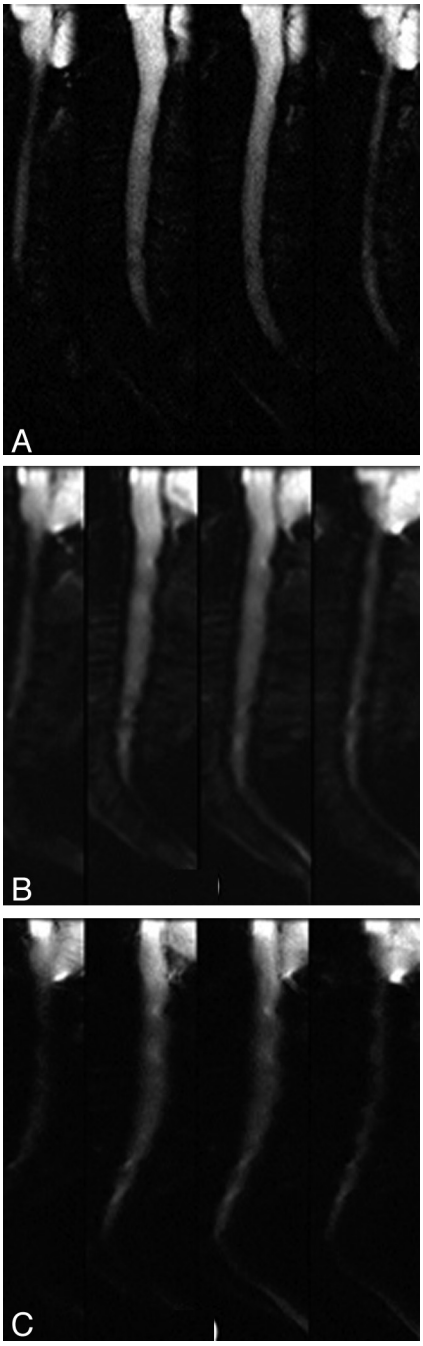

Fig 2. A 71-year-old woman with right-sided weakness and hemifacial spasm. Comparison of DWI by using either rFOV (*A*); fFOV matched to have the same readout time (with subsequently lower spatial resolution) (*B*); or fFOV matched to have the same spatial resolution, with increased readout time (and associated susceptibility artifacts) (*C*). All images were matched for acquisition time (2.5 minutes). Only the 4 central sections are shown. rFOV DWI demonstrates high spatial resolution with minimal artifacts and acceptable SNR.

diskectomy and fusion demonstrates that the susceptibility artifact from the metallic plate is mitigated though not entirely eliminated by the rFOV method (Fig 6).

Discussion

This study demonstrates that a rFOV approach using a 2D RF pulse enables acquisition of high-resolution spinal cord diffusion images with reduced artifacts compared with conventional SS-EPI. By reducing the FOV, it is possible to obtain

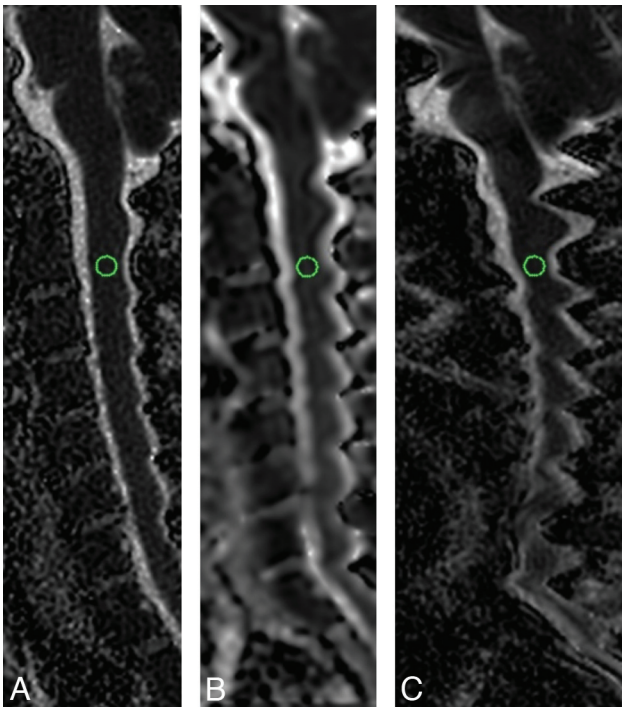

Fig 3. rFOV (*A*), low-resolution fFOV (*B*), and high-resolution fFOV ADC maps (*C*) demonstrating the location of the ROI used for the ADC measurements, placed on the centermost section of the sagittal images at the level of C2–3.

Table 2: Agreement of the 2 reviewers

Measure	Weighted κ	95% CI	Symmetry Test, *P* Value
Susceptibility	0.58	0.48–0.66	.968
Resolution	0.53	0.40–0.63	.767
SNR	0.45	0.35–0.56	.405
Anatomy	0.53	0.42–0.62	.011
Clinical utility	0.59	0.48–0.68	.468

images at a given spatial resolution with a reduced number of *k*-space lines. For single-shot imaging, this directly translates to a shorter readout time and higher (pseudo) bandwidth along the phase-encode dimension; consequently, imaging artifacts such as blurring and pixel misregistration are reduced. The ability to acquire an asymmetric FOV is particularly well suited for sagittal imaging of the spinal cord, given that the relevant anatomic structures are elongated in the superior-inferior direction relative to the AP direction. The current study demonstrates that the combination of higher spatial resolution, decreased imaging artifacts, and good coverage of the relevant anatomy improves spinal cord DWI in clinical patients, as evaluated by 2 experienced neuroradiologists.

Improved anatomic depiction of the spinal cord by using rFOV was most notable in regions immediately ventral to the posterior spinous processes, which were often marred by a significant alteration of perceived AP cord diameter, cord signal intensity, and cord ADC values on the fFOV diffusion images (eg, Fig 5). Also, there were improvements in anatomic fidelity around metal (Fig 6) on the rFOV images. Both readers preferred the rFOV diffusion images to either of the fFOV images in all metrics by using a subjective 5-point scale. This preference was strongest for clinical utility, possibly because it represents the combined effect of the other assessed attributes,

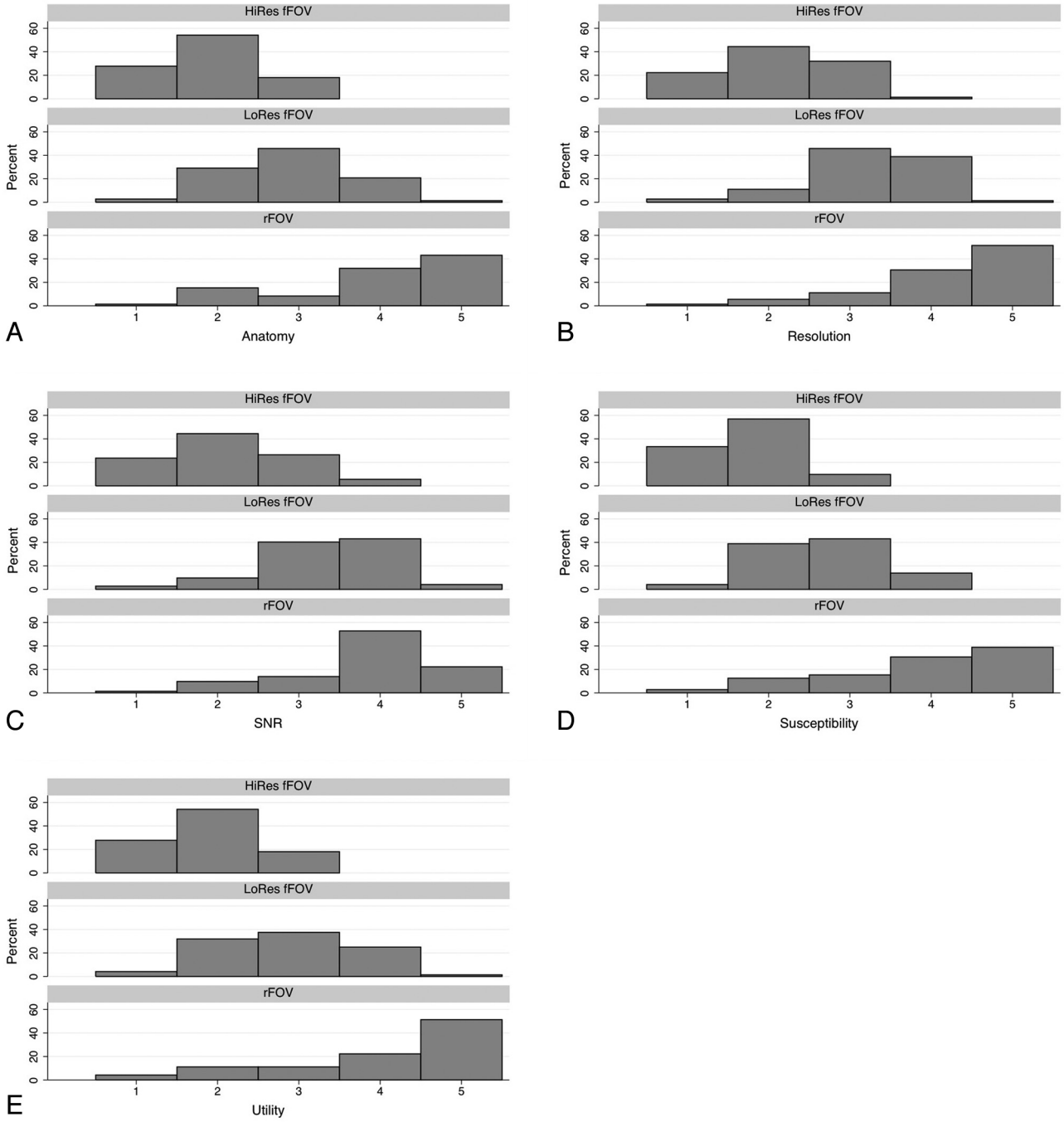

Fig 4. Pooled reviewer ratings of anatomy (*A*), perceived resolution (*B*), perceived SNR (*C*), susceptibility artifact (*D*), and clinical utility (*E*) for each of the 3 assessed sequences: High-resolution fFOV (HiRes fFOV), low-resolution fFOV (LoRes fFOV), and rFOV. All 3 sequences were significantly different from each other on all ratings, with rFOV having consistently higher ratings than the LoRes fFOV sequence, which in turn was preferred over the HiRes fFOV sequence (all calculated *P* values $\leq$ .0001). All values are expressed as a percentage of total responses by both reviewers.

such as improved susceptibility effects, SNR, and spatial resolution. Although still significant, the preference based on SNR of the resultant images was not as strong, with a significant number of the low-resolution fFOV images also deemed good or excellent. One must keep in mind, however, that the voxel size of the low-resolution fFOV images was 4 times larger than the rFOV images. High resolution is critical for imaging of the spinal cord given its small dimensions; when one compares the preference between the rFOV and fFOV images at fixed high spatial resolution, there is strong preference for the rFOV images (Fig 4).

ADC values were measured using the rFOV method in the upper cervical cord and were not statistically different from measurements made with conventional fFOV methods. Mean ADC values were within the range of measurements in previous reports.[1,3,5,24,49,50]

Several factors suggest that rFOV DWI may be a clinically feasible approach to image the spinal cord. The rFOV approach is time-efficient, as evidenced by the short duration (2.5 minutes) of the scans obtained in the current study. Although multishot interleaved methods would be expected to have similar SNR, the combination of data from multiple ac-

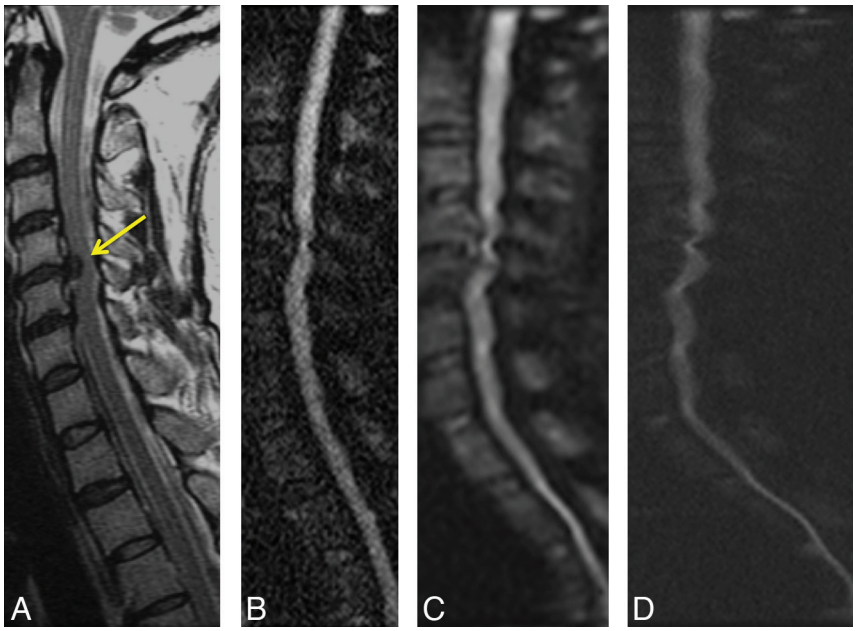

Fig 5. A 42-year-old woman with left-sided arm weakness and multiple posterior disk-osteophyte complexes, the largest of which is located at C4–5 (arrow). Sagittal T2-weighted (*A*), rFOV DWI (*B*), low-resolution fFOV DWI (*C*), and high-resolution fFOV DWI (*D*) are shown. The rFOV diffusion images significantly alleviate susceptibility and partial volume effects that cause pixel misregistration and image warping on the fFOV diffusion scans.

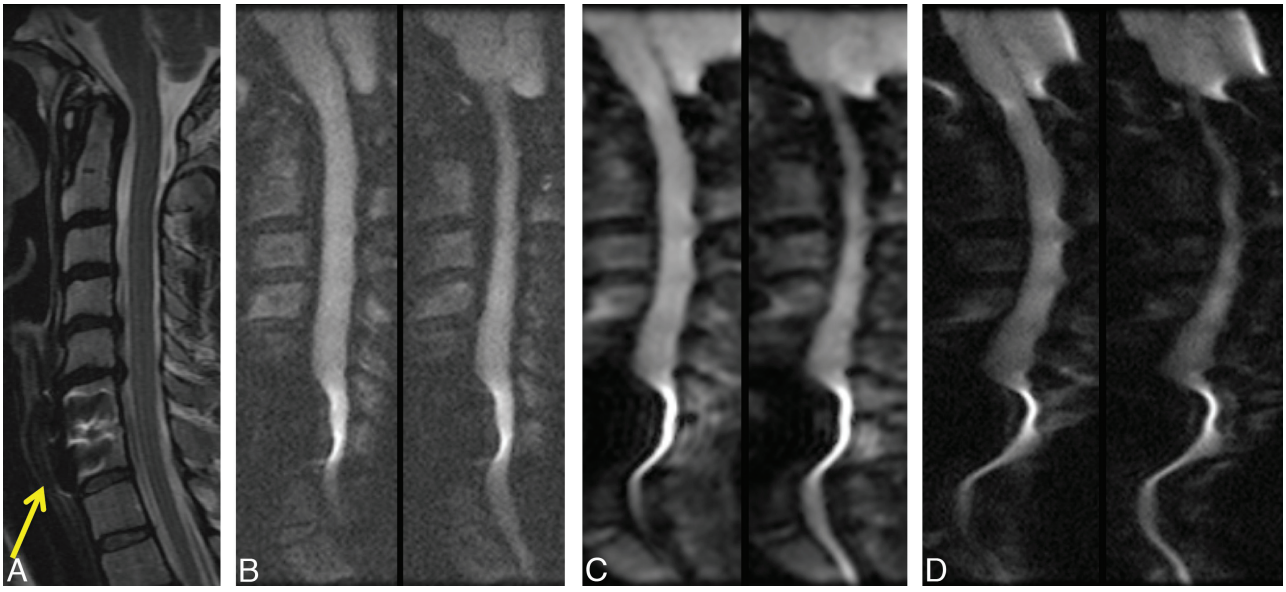

Fig 6. A 40-year-old woman status post C6–7 anterior cervical diskectomy and fusion. Sagittal T2-weighted (*A*), rFOV DWI (*B*), low-resolution fFOV DWI (*C*), and high-resolution fFOV DWI (*D*) are shown. The rFOV diffusion images somewhat mitigate but do not eliminate the metallic artifacts associated with the plate, but they do remain more diagnostically useful than the fFOV diffusion images that are severely distorted.

quisitions is less robust and overall imaging time is increased. Furthermore, because the modification to SS-EPI is only in the excitation pulse, if further improvements in susceptibility artifacts or higher spatial resolution are required, then it can be combined in a straightforward manner with other approaches, including parallel and multishot/interleaved EPI, though at a cost of longer scan time. Another benefit of single-shot acquisition is that by acquiring an entire section in a single excitation, and an entire contiguous volume within a TR interval, rFOV DWI is amenable to both 2D and 3D motion correction methods. Eddy current correction was not applied. This was because a lower *b*-value was used than in the brain. The higher effective bandwidth of rFOV also diminished geometric distortion effects emanating from eddy currents induced from switching diffusion-encoding gradients.

Another approach to acquire an rFOV is to suppress or dephase the signal intensity from tissue outside the desired FOV by using additional RF pulses. These techniques may be contrasted with the rFOV approach used in this study, which, rather than exciting and then suppressing/dephasing such regions, does not excite these regions in the first place. One such method, ZOOM-EPI,[43] relies on a 180° refocusing pulse that is oblique to the initial section, such that only the parallelogram-shaped volume that experiences both the initial 90° and 180°

pulses contributes to the signal intensity during readout; this method was applied to image the spinal cord and the optic nerve, but it cannot be used to acquire contiguous sections without an SNR penalty, because the regions excited by the 2 pulses overlap with the adjacent sections. This is particularly problematic for imaging in the sagittal plane, because the entire spinal cord is only approximately 1 cm wide. Two other methods use refocusing pulses that are selective in the phase-encode direction to readout a rectangular FOV.[44,46] The first method, known as contiguous ZOOM-EPI,[46] uses 2 refocusing pulses such that spins outside the rFOV within contiguous sections are minimally affected; this also has the advantage of limiting eddy current distortions.[51] Another method places this second refocusing pulse immediately after the readout period, resulting in shorter echo times and resultant higher SNR.[44] However, the neighboring sections can still experience an SNR decrease due to T1 recovery between the 2 refocusing pulses. This method has been applied to study diffusion in cervical disk disease[19] and carotid bifurcation atherosclerosis.[52] A final method[47] uses successive outer volume suppression pulses to saturate the signal intensity outside the desired FOV; however, this leads to potentially higher specific absorption rates and the effectiveness of the suppression is sensitive to variations in the transmit B_1 field. In summary, all of these approaches share the need to suppress signal intensity from surrounding tissue, and as such, may be suboptimal in the setting of motion or magnetic field inhomogeneities.

We now point out several limitations to our study. Because sagittal images most efficiently covered the territory of interest with the fewest number of images, we did not routinely acquire or assess axial images. This was largely due to time considerations, because we wanted to acquire multiple diffusion series in a single examination. In the few cases in which we acquired axial sections (eg, On-line Fig 2), however, the images were diagnostic and seemed superior to those obtained typically with fFOV methods. Although the original rFOV method had limitations in that it could only acquire 6–8 sections due to the periodic nature of the rFOV pulse,[45] more recent approaches, including Hadamard encoding[53] and improved 2D RF pulse design, can be used to significantly increase the number of contiguous sections, such that axial imaging of the entire cervical spinal cord with 4-mm contiguous sections would be possible with 2 acquisitions, requiring 5 minutes for the same SNR as the sagittal images. Also, we did not perform a comparison study of the different methods in the thoracic spine, where increased motion, including cardiac, respiratory, and CSF flow, is greater than in the cervical spine. However, our experience in a limited number of patients (eg, On-line Figs 3 and 4) suggests that rFOV performs well in the thoracic spine. This may be due to the greater reductions in the phase-encode FOV due to more elongated contour of the thoracic spine in most individuals.

We chose to examine fFOV diffusion imaging with equivalent section thickness and imaging time. We did not compare with other competing approaches, including multishot interleaved EPI, parallel EPI, or outer volume suppression methods. Also, the fFOV images were acquired only by using a standard square FOV SS-EPI sequence. Even with a nonselective excitation pulse, it may be possible to read out a slightly rectangular FOV with minimal aliasing artifacts due to the geometry of the cervical spine. Placement of anterior saturation bands also would reduce aliasing and breathing artifacts with this approach. We did not choose to optimize the fFOV DWI scans in this manner, because this has not been part of our traditional clinical routine. Thus, the advantages of the rFOV approach that we describe may be less apparent if somewhat more optimized diffusion imaging methods are considered as the standard.

We did not perform DTI as part of this study; thus, we cannot report on longitudinal and parallel ADC values or fractional anisotropy. However, there is no inherent limitation in the sequence for DTI,[54] and it was omitted in the current study only because our goal was to assess overall image quality rather than these other metrics. Improved anatomic fidelity and high spatial resolution in the underlying diffusion images is critical for DTI studies in the spinal cord, and this topic will be a subject of future studies.

Finally, only relatively mild abnormalities were noted on these clinical studies, limited to degenerative disk disease; specifically, no diffusion abnormalities were observed on any of the studies. This is in keeping with the relatively uncommon nature of spinal cord infarction and other pathologies in the typical patient population referred for cervical spine examinations. However, our clinical experience suggests that the method aids in the detection of pathology, as demonstrated in the case of thoracic spinal cord infarction shown in On-line Fig 4. In future reports, we plan to describe in a more comprehensive manner the findings of rFOV DWI in a larger group of patients that includes such pathologies, but does not receive comparison fFOV SS-EPI, to allow us to comment on important issues such as lesion conspicuity.

Conclusions

Reduced FOV spinal cord DWI is feasible in a clinical population, improves image quality, and is preferred over conventional fFOV SS-EPI in a clinical population. Further studies to assess conspicuity and clinical utility for visualizing commonly encountered spinal cord pathologies are warranted.

Acknowledgments

We thank Dr. Roland Bammer, PhD, for helpful comments and discussions during the preparation of this manuscript.

References

1. Holder CA. **MR diffusion imaging of the cervical spine.** *Magn Reson Imag Clin N Am* 2000;8:675–86
2. Melhem ER. **Technical challenges in MR imaging of the cervical spine and cord.** *Magn Reson Imag Clin N Am* 2000;8:435–52
3. Clark CA, Barker GJ, Tofts PS. **Magnetic resonance diffusion imaging of the human cervical spinal cord in vivo.** *Magn Reson Med* 1999;41:1269–73
4. Bammer R, Augustin M, Prokesch RW, et al. **Diffusion-weighted imaging of the spinal cord: interleaved echo-planar imaging is superior to fast spin-echo.** *J Magn Reson Imaging* 2002;15:364–73
5. Bammer R, Fazekas F. **Diffusion imaging of the human spinal cord and the vertebral column.** *Top Magn Reson Imaging* 2003;14:461–76
6. Ciccarelli O, Wheeler-Kingshott CA, McLean MA, et al. **Spinal cord spectroscopy and diffusion-based tractography to assess acute disability in multiple sclerosis.** *Brain* 2007;130:2220–31
7. Farrell JA, Smith SA, Gordon-Lipkin EM, et al. **High b-value q-space diffusion-weighted MRI of the human cervical spinal cord in vivo: feasibility and application to multiple sclerosis.** *Magn Reson Med* 2008;59:1079–89
8. van Hecke W, Nagels G, Emonds G, et al. **A diffusion tensor imaging group study of the spinal cord in multiple sclerosis patients with and without T2 spinal cord lesions.** *J Magn Reson Imaging* 2009;30:25–34

9. Hesseltine SM, Law M, Babb J, et al. **Diffusion tensor imaging in multiple sclerosis: assessment of regional differences in the axial plane within normal-appearing cervical spinal cord.** *AJNR Am J Neuroradiol* 2006;27:1189–93
10. Loher TJ, Bassetti CL, Lovblad KO, et al. **Diffusion-weighted MRI in acute spinal cord ischaemia.** *Neuroradiology* 2003;45:557–61
11. Sagiuchi T, Iida H, Tachibana S, et al. **Case report: diffusion-weighted MRI in anterior spinal artery stroke of the cervical spinal cord.** *J Comput Assist Tomogr* 2003;27:410–14
12. Kuker W, Weller M, Klose U, et al. **Diffusion-weighted MRI of spinal cord infarction–high resolution imaging and time course of diffusion abnormality.** *J Neurol* 2004;251:818–24
13. Shinoyama M, Takahashi T, Shimizu H, et al. **Spinal cord infarction demonstrated by diffusion-weighted magnetic resonance imaging.** *J Clin Neurosci* 2005;12:466–68
14. Thurnher MM, Bammer R. **Diffusion-weighted MR imaging (DWI) in spinal cord ischemia.** *Neuroradiology* 2006;48:795–801
15. Beslow LA, Ichord RN, Zimmerman RA, et al. **Role of diffusion MRI in diagnosis of spinal cord infarction in children.** *Neuropediatrics* 2008;39:188–91
16. Tsuchiya K, Katase S, Fujikawa A, et al. **Diffusion-weighted MRI of the cervical spinal cord using a single-shot fast spin-echo technique: findings in normal subjects and in myelomalacia.** *Neuroradiology* 2003;45:90–94
17. Mamata H, Jolesz FA, Maier SE. **Apparent diffusion coefficient and fractional anisotropy in spinal cord: age and cervical spondylosis-related changes.** *J Magn Reson Imaging* 2005;22:38–43
18. Thurnher MM, Law M. **Diffusion-weighted imaging, diffusion-tensor imaging, and fiber tractography of the spinal cord.** *Magn Reson Imag Clin N Am* 2009;17:225–44
19. Kim TH, Zollinger L, Shi XF, et al. **Quantification of diffusivities of the human cervical spinal cord using a 2D single-shot interleaved multisection inner volume diffusion-weighted echo-planar imaging technique.** *AJNR Am J Neuroradiol* 2010;31:682–87
20. Sagiuchi T, Tachibana S, Endo M, et al. **Diffusion-weighted MRI of the cervical cord in acute spinal cord injury with type II odontoid fracture.** *J Comput Assist Tomogr* 2002;26:654–56
21. Schwartz ED, Hackney DB. **Diffusion-weighted MRI and the evaluation of spinal cord axonal integrity following injury and treatment.** *Exp Neurol* 2003;184:570–89
22. Shen H, Tang Y, Huang L, et al. **Applications of diffusion-weighted MRI in thoracic spinal cord injury without radiographic abnormality.** *International Orthopaedics* 2007;31:375–83
23. Facon D, Ozanne A, Fillard P, et al. **MR diffusion tensor imaging and fiber tracking in spinal cord compression.** *AJNR Am J Neuroradiol* 2005;26:1587–94
24. Ries M, Jones RA, Dousset V, et al. **Diffusion tensor MRI of the spinal cord.** *Magn Reson Med* 2000;44:884–92
25. Murphy BP, Zientara GP, Huppi PS, et al. **Line scan diffusion tensor MRI of the cervical spinal cord in preterm infants.** *J Magn Reson Imaging* 2001;13:949–53
26. Wheeler-Kingshott CA, Hickman SJ, Parker GJ, et al. **Investigating cervical spinal cord structure using axial diffusion tensor imaging.** *Neuroimage* 2002;16:93–102
27. Maier SE, Mamata H. **Diffusion tensor imaging of the spinal cord.** *Ann N Y Acad Sci* 2005;1064:50–60
28. Tsuchiya K, Fujikawa A, Suzuki Y. **Diffusion tractography of the cervical spinal cord by using parallel imaging.** *AJNR Am J Neuroradiol* 2005;26:398–400
29. Lee JW, Kim JH, Kang HS, et al. **Optimization of acquisition parameters of diffusion-tensor magnetic resonance imaging in the spinal cord.** *Invest Radiol* 2006;41:553–59
30. Farzaneh F, Riederer SJ, Pelc NJ. **Analysis of T2 limitations and off-resonance effects on spatial resolution and artifacts in echo-planar imaging.** *Magn Reson Med* 1990;14:123–39
31. Cohen MS, Weisskoff RM. **Ultra-fast imaging.** *Magn Reson Imag* 1990;9:1–37
32. Gudbjartsson H, Maier SE, Mulkern RV, et al. **Line scan diffusion imaging.** *Magn Reson Med* 1996;36:509–19
33. Maier SE, Gudbjartsson H, Patz S, et al. **Line scan diffusion imaging: characterization in healthy subjects and stroke patients.** *Am J Roentgenol* 1998;171:85–93
34. Bammer R, Herneth AM, Maier SE, et al. **Line scan diffusion imaging of the spine.** *AJNR Am J Neuroradiol* 2003;24:5–12
35. Kubicki M, Maier SE, Westin CF, et al. **Comparison of single-shot echo-planar and line scan protocols for diffusion tensor imaging.** *Acad Radiol* 2004;11:224–32
36. Pipe JG, Farthing VG, Forbes KP. **Multishot diffusion-weighted FSE using PROPELLER MRI.** *Magn Reson Med* 2002;47:42–52
37. Fellner C, Menzel C, Fellner FA, et al. **BLADE in sagittal T2-weighted MR imaging of the cervical spine.** *AJNR Am J Neuroradiol* 2010;31:674–81
38. Larson PE, Lustig MS, Nishimura DG. **Anisotropic field-of-view shapes for improved PROPELLER imaging.** *Magn Reson Imaging* 2009;27:470–79
39. Zhang J, Huan Y, Qian Y, et al. **Multishot diffusion-weighted imaging features in spinal cord infarction.** *J Spinal Disorders Techn* 2005;18:277–82
40. Bammer R, Stollberger R, Augustin M, et al. **Diffusion-weighted imaging with navigated interleaved echo-planar imaging and a conventional gradient system.** *Radiology* 1999;211:799–806
41. Cercignani M, Horsfield MA, Agosta F, et al. **Sensitivity-encoded diffusion tensor MR imaging of the cervical cord.** *AJNR Am J Neuroradiol* 2003;24:1254–56
42. Holdsworth SJ, Skare S, Newbould RD, et al. **Readout-segmented EPI for rapid high resolution diffusion imaging at 3 T.** *Eur J Radiol* 2008;65:36–46
43. Wheeler-Kingshott CA, Parker GJ, Symms MR, et al. **ADC mapping of the human optic nerve: increased resolution, coverage, and reliability with CSF-suppressed ZOOM-EPI.** *Magn Reson Med* 2002;47:24–31
44. Jeong EK, Kim SE, Guo J, et al. **High-resolution DTI with 2D interleaved multislice reduced FOV single-shot diffusion-weighted EPI (2D ss-rFOV-DWEPI).** *Magn Reson Med* 2005;54:1575–79
45. Saritas EU, Cunningham CH, Lee JH, et al. **DWI of the spinal cord with reduced FOV single-shot EPI.** *Magn Reson Med* 2008;60:468–73
46. Dowell NG, Jenkins TM, Ciccarelli O, et al. **Contiguous-slice zonally oblique multislice (CO-ZOOM) diffusion tensor imaging: examples of in vivo spinal cord and optic nerve applications.** *J Magn Reson Imaging* 2009;29:454–60
47. Wilm BJ, Svensson J, Henning A, et al. **Reduced field-of-view MRI using outer volume suppression for spinal cord diffusion imaging.** *Magn Reson Med* 2007;57:625–30
48. Kuhl CK, Gieseke J, von Falkenhausen M, et al. **Sensitivity encoding for diffusion-weighted MR imaging at 3.0 T: intraindividual comparative study.** *Radiology* 2005;234:517–26
49. Bammer R, Fazekas F, Augustin M, et al. **Diffusion-weighted MR imaging of the spinal cord.** *AJNR Am J Neuroradiol* 2000;21:587–91
50. Holder CA, Muthupillai R, Mukundan S, et al. **Diffusion-weighted MR imaging of the normal human spinal cord in vivo.** *AJNR Am J Neuroradiol* 2000;21:1799–806
51. Reese TG, Heid O, Weisskoff RM, et al. **Reduction of eddy-current-induced distortion in diffusion MRI using a twice-refocused spin echo.** *Magn Reson Med* 2003;49:177–82
52. Kim SE, Jeong EK, Shi XF, et al. **Diffusion-weighted imaging of human carotid artery using 2D single-shot interleaved multislice inner volume diffusion-weighted echo planar imaging (2D ss-IMIV-DWEPI) at 3T: diffusion measurement in atherosclerotic plaque.** *J Magn Reson Imaging* 2009;30:1068–77
53. Saritas EU, Lee D, Shankaranarayan A, et al. **Hadamard slice-encoding for reduced-FOV single-shot diffusion-weighted EPI.** In: Proceedings of the International Society of Magnetic Resonance in Medicine 2010; Stockholm, Sweden:4355
54. Saritas EU, Zaharchuk G, Shankaranarayan A, et al. **High-resolution DTI tractography of the spinal cord with reduced-FOV single-shot EPI at 3T.** In: Proceedings of the International Society of Magnetic Resonance in Medicine 2010; Stockholm, Sweden:4370